J3.4

RAMAN LIDAR: A VERSATILE REMOTE SENSING INSTRUMENT FOR WATER VAPOR AND CIRRUS CLOUD STUDIES

Thomas P. Ackerman[1]*, Jennifer M. Comstock[1], and David D. Turner[1,2]
1 Pacific Northwest National Laboratory, Richland WA
2 University of Wisconsin, Madison WI

1. INTRODUCTION

The Department of Energy's Atmospheric Radiation Measurement (ARM) program has operated a Raman lidar at the Southern Great Plains site in northern Oklahoma nearly continuously since April 1998, collecting over 20,000 hours of data in all seasons under a wide range of atmospheric conditions. This Raman lidar measures the elastic and Raman backscatter from molecules, aerosols, and cloud particles at multiple wavelengths. These signals are then processed to yield profiles of water vapor mixing ratio, relative humidity, aerosol extinction, aerosol backscatter, linear depolarization ratio, and cloud boundaries. Raman lidars are able to measure the aerosol extinction and backscatter directly, and thus no assumptions are required (as for single wavelength lidars) to retrieve these products.

The physical properties of clouds (such as the location, vertical distribution, particle size and shape, etc.) dictate the radiative impact of the clouds on climate. Cirrus cloud properties are difficult to observe, given their typical atmospheric altitude, and thus there is large uncertainty in the radiative feedback of these clouds. The Raman lidar measurements are being used to quantify the properties of these clouds. The Raman lidar is able to measure upper tropospheric humidity with approximately 5% absolute accuracy (Ferrare et al. 2003), and thus the linkage between ice supersaturation and cirrus formation and persistence can be examined. The ratio of the aerosol backscatter to aerosol extinction in clouds is related to the backscatter phase function of the cloud particles. Using this ratio in conjunction with the linear depolarization ratio, there is potential for ascertaining the ice crystal shape from lidar measurements. Here, we illustrate the Raman lidar capability and apply this capability to the study of cirrus cloud properties at the Oklahoma ARM site.

2. THE RAMAN TECHNIQUE

The ARM Raman lidar (RL) (Goldsmith et al. 1998; www.arm.gov) measures profiles of extinction (α) and backscatter (β) coefficient due to aerosols, water vapor and clouds in the atmosphere. The RL transmits a laser pulse at 355 nm (λ_o), which undergoes elastic scattering due to clouds and aerosols. In addition to elastically scattered photons, the RL detector also receives inelastic scattered photons that allow for the detection of specific molecules in the atmosphere, which for the ARM Raman lidar includes nitrogen (N_2) at 387 nm and water vapor at 408 nm. Inelastic scattering arises when the transmitted laser pulse excites a vibrational as well as an electronic transition in a molecule. When the molecule relaxes to its electronic ground state but an excited vibrational state, the scattered photon emerges at a slightly reduced energy and longer wavelength. This wavelength shift produced by Raman scattering is uniquely identified with a particular molecule. Consequently, it can be used to produce high temporal resolution vertical profiles of water vapor. The water vapor mixing ratio is proportional to the ratio of the water vapor and nitrogen signals, which are measured simultaneously.

The RL estimates vertical profiles of backscatter and extinction due to aerosols and cloud particles in the atmosphere. In this study, we estimate particle extinction coefficient at 355 nm using (Ansmann et al. 1992)

$$\alpha(z) = \frac{\frac{d}{dz}\left[\ln \frac{N_R(z)}{P_{\lambda_R}(z)z^2}\right] - \alpha_{\lambda_o}^{mol}(z) - \alpha_{\lambda_R}^{mol}(z)}{1+\left(\frac{\lambda_o}{\lambda_R}\right)^l} \qquad (1)$$

where λ_R denotes the nitrogen 387 nm wavelength, N_R is the N_2 molecular number denstiy, P_{λ_R} is the N_2 Raman backscatter signal and α_{mol} is the molecular extinction coefficient. The parameter *l*=1 for aerosols and water droplets, and *l*=0 for large particles such as ice crystals.

The particle backscatter coefficient is derived from the total scattering ratio (TSR), which is the ratio of the total (molecular plus particle) to molecular scattering. The parameter TSR includes scattering from aerosols, water droplets, and ice crystals. Once TSR is determined, β is calculated using

$$\beta(z) = [TSR(z)-1]\sigma_R \rho(z)\frac{3}{8\pi} \qquad (2)$$

where σ_R is the Rayleigh cross section at 355 nm and $\rho(z)$ is the molecular number density. The backscatter-to-extinction ratio (*k*) is simply the ratio of β and α. Turner et al. (2002) discuss details concerning the calculation of water vapor mixing ratio and α, where uncertainties are listed as 5% and 10%, respectively.

The returned energy at λ_o is separated into both co-polarized ($P_{||}$) and cross-polarized ($P_{\perp}$) returns

* Corresponding author address: Thomas P. Ackerman, PNNL, MSIN K9-34, Richland, WA, 99352; email: ackerman@pnl.gov

(with respect to the polarization of the outgoing laser beam). The depolarization ratio ($\delta = P_{\perp} / P_{\parallel}$) is useful for determining cloud phase and, to some extent, ice crystal shape and orientation.

3. WATER VAPOR AND AEROSOL MEASUREMENTS

High resolution water vapor and aerosol profile measurements can improve our understanding of the role of water vapor and ice supersaturation in cloud formation, radiative flux calculations, and water vapor-aerosol interactions. Boundary layer water vapor can vary significantly between typical 12 hour radiosonde profiles. Measurements from 20 March 2000, a nearly cloudless day, reveal distinct variations in water vapor (Fig. 1b). Over this same time period, we estimate the aerosol optical thickness from the aerosol extinction coefficient (Fig. 1a and c).

Several studies of aerosol and water vapor over the ARM SGP site have been conducted using the Raman lidar. One study examined 7500 h of RL data and show that aerosol extinction varies with both season and time of day, with a maximum aerosol optical thickness (τ_a) observed in the summer (Turner et al. 2001). The same study also shows that during summer months, aerosols can extend up to ~6 km, which is well above the boundary layer. Aerosol size and composition can also be studied using the aerosol backscatter-to-extinction ratio (k_a). Ferrare et al. (2001) show that although τ_a varies seasonally, k_a does not. However, k_a does vary significantly with height and as aerosol composition changes. For example, k_a increases are correlated with smoke advecting over the SGP site (Peppler et al. 2000).

4. UPPER TROPOSPHERIC CLOUDS

The ARM Raman lidar was designed to primarily study water vapor and aerosols in the lower troposphere. Therefore, a large portion of the N_2 signal is discarded so that the signal received in the boundary layer (where the majority of the water vapor lies) remains in the linear range of the detectors. This signal degradation limits retrievals of upper tropospheric clouds to times when the signal-to-noise ratio (SNR) is high. Because the solar background energy increases noise, measurements of water vapor during daytime hours are limited to below 4 km. (This aspect of the RL can be overcome but requires some additional engineering of the system that has not yet been done.) However, during the night, water vapor profile measurements can extend to 12 km, which allows for studies of relative humidity (RH) variations in the upper troposphere (UT).

The exact physics of cirrus cloud formation and maintenance in the upper troposphere is not well understood. Cloud-resolving model studies typically find that formation is linked to large ice supersaturation at high altitudes, coupled with some amount of vertical lifting (Jensen et al. 2001). Large-scale model parameterizations general attempt to link cirrus formation and ice water amount to some combination of UT temperature, UT relative humidity, and vertical motion. Mace et al. (2001) used millimeter-wavelength radar data and weather model analyses to investigate these relationships. They found a modest correlation between ice water content with temperature but little correlation with large-scale vertical ascent. Part of this lack of correlation may be due to the fact that their study did not include water vapor amount as a variable. UT RH is difficult to measure at the resolution required for such studies because traditional radiosonde measurements are typically unreliable for temperatures below –35°C or – 40°C. The RL provides these measurements during night hours.

Using RL water vapor profiles, we estimate RH with respect to ice (RH_{ice}) during the night at cirrus altitudes (Fig. 2a). A height vs. time display of linear depolarization ratio indicates that cirrus clouds exist in this region of supersaturated air only a small fraction of the time (Fig. 2b). However, in a different case (Fig. 3), cirrus clouds exist nearly the entire day under supersaturated conditions. In order to obtain the vertical velocity for these cases, we use the results of the Constrained Variational Analysis (CVA; Zhang and Lin 1997; Zhang et al. 2001) performed for the ARM SGP site. The CVA technique uses a combination of weather model analysis and ARM SGP data, such as radiosonde profiles and thermal and microwave radiances, along with variational mathematics to determine the large-scale state of the atmosphere across the SGP site. The CVA provides as one of its outputs, the vertical velocity on the scale of tens of kilometers. The CVA indicates overall upwelling on 16 February 2000 and subsidence for the 7 December 2000 case. These cases suggest that we can use the combination of the RL measurements of cirrus extinction and UT RH along with the CVA vertical velocity to investigate the relationship between cirrus life cycle and upper troposphere meteorology.

Profiles of α, k, and δ (Figs. 2 and 3) can provide insight into cirrus microphysical properties and cloud phase determination. Vertical variations in cloud extinction have significant impact on radiative flux and heating rate calculations, which can affect cirrus cloud model simulations (Khvorostyanov and Sassen 1998). Subgrid-scale variations in cirrus cloud microphysical properties will also contribute to a solar albedo bias in global circulation models (GCMs). Neglecting subgrid-scale variability will cause an overestimation of solar albedo over low reflective surfaces and an underestimation over highly reflective surfaces (Carlin et al. 2002).

By combining k and δ, there is a potential to discern ice crystal shape in cirrus clouds. The parameter k is equivalent to the normalized scattering phase function at 180°, which depends

on both ice crystal shape and size. Depolarization ratio also varies with both shape and cloud phase. For example, spherical particles, such as water droplets, have low depolarization, while ice crystals display depolarization, typically between 20 and 40% in midlatitude cirrus clouds (Sassen and Benson 2001). There is some evidence that certain ice crystal shapes tend to grow in certain temperature (T) ranges. Therefore, theoretically one would expect to see some correlation between k, δ, and T. However, Raman lidar measurements from SGP in 2000 do not exhibit a clear relationship between k, δ, and T (Fig. 4). There is a slight increase in δ with decreasing T, which agrees with other studies (Platt et al. 1998; Sassen and Benson 2001). Since cirrus clouds are composed of mixtures of ice crystal habits and sizes, which are generally randomly oriented, the weak relationship between k, δ, and T is not surprising.

5. DISCUSSION

In this paper, we provide a general overview of Raman lidar capabilities for studying water in various phases present in the atmosphere. RL vertical profiles of water vapor mixing ratio provide important information at high spatial and temporal resolution concerning the variation of water vapor in the atmosphere and its relationship to cloud formation. The RL is also capable of directly measuring profiles of aerosol and cloud extinction, which are important in radiative transfer calculations. Ice supersaturation in the upper troposphere, essential in studying cirrus formation and persistence, is also measured to approximately 5% accuracy during the nighttime.

Although this analysis of k and δ does not reveal clear relationships with temperature, there may be some dependency if data were divided according to season or cirrus generating mechanism. This topic will be addressed in future studies.

The ARM data are available through the ARM data archive for use by any interested scientist. Information regarding ARM and access to the data can be found at the arm web site, http://www.arm.gov.

6. ACKNOWLEDGEMENTS

The Pacific Northwest National Laboratory is operated by Battelle for the U. S. Department of Energy (DOE). This research was supported by the DOE Office of Biological and Environmental Research under contract number DE-AC06-76RL01830 as part of the Atmospheric Radiation Measurement Program.

7. REFERENCES

Ansmann, A., U. Wandinger, M. Riebesell, C. Weitkamp, and W. Michaelis, 1992: Independent measurement of extinction and backscatter profiles in cirrus clouds by using a combined Raman elastic-backscatter lidar. *Appl. Opt*., **31**, 7113-7131.

Carlin, B., Q. Fu, U. Lohmann, G. G. Mace, K. Sassen, and J. M. Comstock, 2002: High-cloud horizontal inhomogeneity and solar albedo bias. *J. Climate*, **15**, 2321-2339.

Ferrare, R. A., D. D. Turner, L. H. Brasseur, W. F. Feltz, O. Dubovik, and T. P. Tooman, 2001: Raman lidar measurements of the aerosol extinction-to-backscatter ratio over the Southern Great Plains. *J. Geophys. Res*., **106**, 2033-20347.

R. A. Ferrare, E. Browell, S. Ismail, S. Kooi, L. H. Brasseur, V. G. Brackett, M. Clayton, J. Barrick, H. Linne, A. Lammert, G. Diskin, J. Goldsmith, B. Lesht, J. Podolske, G. Sachse, F. Schmidlin, D. Turner, D. Whiteman, and L. Miloshevich, 2003: Lidar characterizations of water vapor measurements over the ARM SGP site. *Symposium on observing and understanding the variability of water and climate*, *AMS Annual Meeting, Long Beach CA*.

Goldsmith, J. E. M., F. H. Blair, S. E. Bisson, and D. D. Turner, 1998: Turn-key Raman lidar for profiling atmospheric water vapor, clouds, and aerosols. *Appl. Opt*., **37**, 4979-4990.

Jensen, E. J., O. B. Toon, S. A. Vay, J. Ovarlez, R. May, T. P. Bui, C. H. Twohy, B. W. Gandrud, R. F. Pueschel, and U. Schumann, 2001: Prevalence of ice-supersaturated regions in the upper troposphere: implications for optically thin ice cloud formation. *J. Geophys. Res*., **106**, 17253-17266.

Khvorostyanov, V. I., and K. Sassen, 1998: Cirrus cloud simulation using explicit microphysics and radiation. Part II: microphysics, vapor and ice mass budgets, and optical and radiative properties. *J. Atmos. Sci.*, **55**, 1822-1845.

Mace, G. G., E. E. Clothiaux, and T. P. Ackerman, 2001: The composite characteristics of cirrus clouds: Bulk properties revealed by one year of continuous cloud radar data. *J. Climate*, **14**, 2185-2203.

Peppler, R. A., C. P. Bahrmann, J. C. Barnard, J. R. Campbell, M.-D. Cheng, R. A. Ferrare, R. N. Halthore, L. A. Heilman, D. L. Hlavka, N. S. Laulainen, C.-J. Lin, J. A. Ogren, M. R. Poellot, L. A. Remer, K. Sassen, J. D. Spinhirne, M. E. Splitt, and D. D. Turner, 2000: ARM Southern Great Plains site observations of the smoke pall associated with the 1998 Central American fires. *Bull. Amer. Metero. Soc*., **81**, 2563-2591.

Platt, C. M. R., S. A. Young, P. J. Manson, G. R. Patterson, S. C. Marsden, R. T. Austin, and J. H. Churnside, 1998: The optical properties of equatorial cirrus from observations in the ARM Pilot Radiation Observation Experiment. *J. Atmos. Sci.*, **55**, 1977-1996.

Sassen, K., and S. Benson, 2001: A midlatitude cirrus cloud climatology from the Facility for Atmospheric Remote Sensing. Part II:

microphysical properties derived from lidar depolarization. *J. Atmos. Sci.*, **58**, 2103-2112.

Turner, D. D., R. A. Ferrare, L. A. Brasseur, 2001: Average aerosol extinction and water vapor profiles over the southern great plains. *Geophys. Res. Let.*, **28**, 4441-4444.

Turner, D. D., R. A. Ferrare, L. A. H. Brasseur, W. F. Feltz, T. P. Tooman, 2002: Automated retrieals of water vapor and aerosol profiles from an operational raman lidar. *J. Atmos. Oceanic Tech.*, **19**, 37-50.

Zhang, M.H. and J.L. Lin, 1997: Constrained variational analysis of sounding data based on column-integrated conservations of mass, heat, moisture, and momentum: Approach and application to ARM measurements. *J. Atmos. Sci.*, **54**, 1503-1524.

Zhang, M.H., J.L. Lin, R.T. Cederwall, J.J. Yio, and S.C. Xie, 2001: Objective analysis of ARM IOP data: Method and sensitivity. *Mon. Wea. Rev.*, **129**, 295-311.

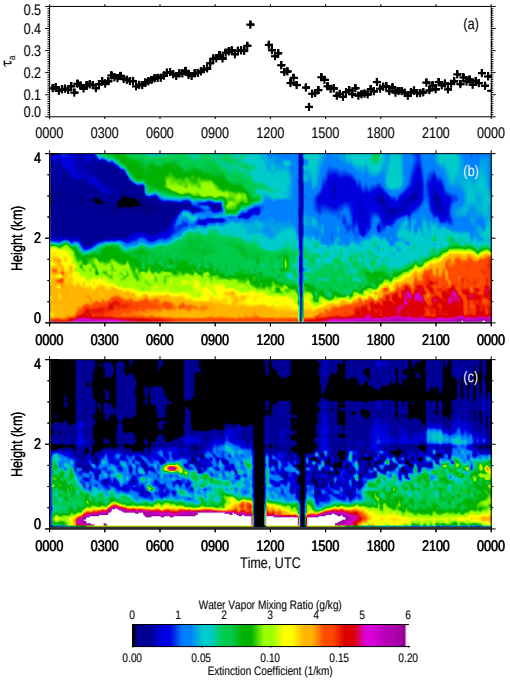

Figure 1. (a) Aerosol optical thickness, (b) water vapor mixing ratio, and (c) aerosol extinction coefficient measured by the Raman lidar on 20 March 2000. Temporal and vertical resolutions are 10 min and 78 m, respectively.

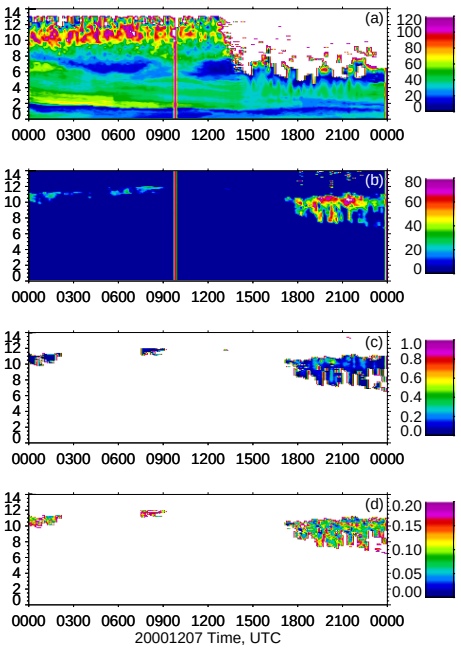

Figure 2. (a) RH_{ice} (%), (b) depolarization ratio (%), (c) extinction (km^{-1}), and (d) backscatter-to-extinction ratio (sr^{-1}) measured on 7 Dec 2000.

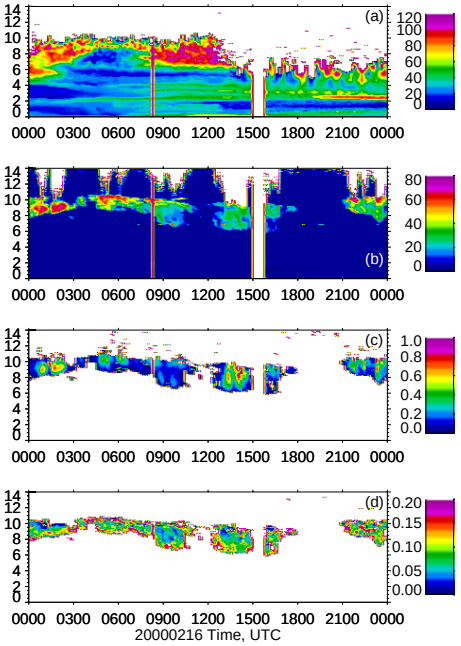

Figure 3. (a) RH_{ice} (%), (b) depolarization ratio (%), (c) extinction (km^{-1}), and (d) backscatter-to-extinction ratio (sr^{-1}) measured on 16 February 2000.

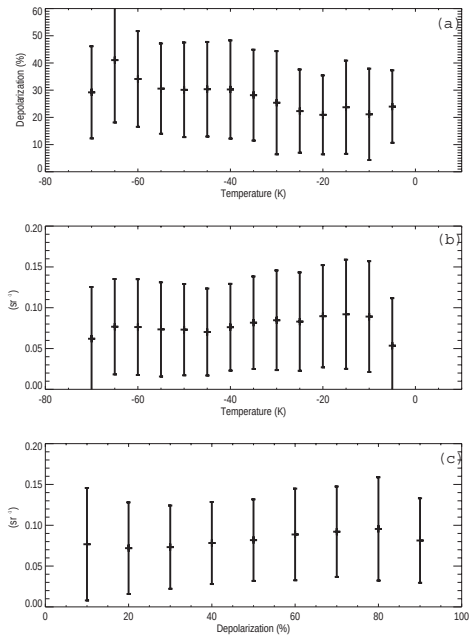

Figure 4. (a) Depolarization ratio and (b) backscatter-to-extinction ratio averaged over 5°C temperature intervals. Temperature is taken from radiosonde measurements. (c) Backscatter-to-extinction ratio averaged over depolarization ratio in 10% intervals. All plots are compiled measurements from 2000 at SGP.